ISSN: 0369-8963

CO_2 Laser Study of SS316 and Ni201 Dissimilar Metal Joining

G. KRISHNA KUMAR[A*], C.VELMURUGAN[B], T. KANNAN[C] R.S. JAYARAM[D]

[a]Department of Mechatronics Engineering, Nehru Institute of Engineering and Technology, Coimbatore, Tamilnadu, India.

[b]Department of Mechanical Engineering, Kumaraguru College of Technology, Coimbatore, Tamilnadu, India.

[c]Department of Mechanical Engineering, SVS College of Engineering, Coimbatore, Tamilnadu, India.

[d]Department of Mechanical Engineering, Amrita College of Engineering and Technology, Nagercoil, Tamilnadu, India.

**Corresponding author Email: gkknehru@gmail.com*

Abstract

Dissimilar metal welded joints are commonly used in the nuclear sector to connect pressure vessel ferritic steel pipe nozzles to austenitic stainless steel safe-end pipes. Stainless Steel 316 and Nickel 201 dissimilar joints are focused on by utilising a 4KW CO_2 laser welding machine in this study. Mechanical parameters such as ultimate tensile strength (UTS) and hardness survey were used to identify a high-quality welded junction. The tensile stress was found to be 412 Mpa, and the fracture occurred outside the weld zone on the nickel side. The tensile test shows that the weld was strong enough to break through the base metal. The profile of the weld bead is critical to ensure that it is a strong weld junction. Some delta ferrite has been observed in the interdendritic zone in microstructure studies, along with columnar grains during solidification, all of which point to successful fusing in the joint between the two dissimilar metals. With the 4 kW CO_2 laser welding machine, it is possible to join materials that are completely different from each other.

Keywords: *CO_2 Laser, Dissimilar Metal Weld Joint, SS 316, Nickel 201, Mechanical Properties, Microstructure*

Introduction

Laser welding is the most accurate method for connecting different materials. Laser beam welding is a superior joint and its strength-to-size ratio is excellent. Its uniformity and heat impacted zone are minimal. Nickel and stainless steel are two prevalent materials that are becoming increasingly used in aerospace, nuclear power plants, and food processing industries. Steel and nickel joints welded together with dissimilar metals require a fix during the section assembly process. Focused high power density beams [1–5] overcome the common fusion problems caused by varying thermal conductivity. It was found that base metals Inconel 600 and

 https://doi.org/10.37896/pd91.4/91419

ISSN: 0369-8963

Inconel 690 were not adversely impacted by welding heat, and that they obtained satisfactory tensile and shear strength. The welding of complex structures in nuclear power plants is made possible by the Nd: YAG laser's unique properties [6, 7]. In addition to saving energy by reflection, a keyhole design extends heat to the metal underneath through thermal conduction, making it even more efficient. Maintaining a nominal metal-to-metal distance should be a top priority. If the material's surface melting power is extremely low [8–10], the CO_2 laser welding solves the frequent residual stress problem when dissimilar metals are joined, even if the metals have different coefficients of thermal expansion and heat conductivity. These two parameters, welding speed and laser power, had the greatest impact on the fusion area. The laser energy input is determined by a carefully orchestrated mix of the welding process's many parameters and controls. In order to regulate the output characteristics of a laser welder, focus size, shielding gas, laser power, and welding speed were critical. Analysis of metal microstructure and composition at different scanning speeds was used to investigate a copper-nickel dissimilar pair. They blended well with one another. Weld pools were stretched because of the influence of thermal characteristics. [11] Carlson concentrated on the link between the heat input and the depth of penetration of the laser beam welding. As soon as the power density reaches a certain threshold, a hollow is formed in the material. Perfect penetration is achieved with the least amount of heat input by using the optimum laser power and welding speed. Laser welding for stainless steel, nickel alloys, and titanium alloys was tested [12–15].

An Electron Diffraction Scanning Microscopy (EDS) study of CO_2 laser welded dissimilar metal joints demonstrated effective mixing and solidification of SS and Cu. A 10 mm thick HAZ was discovered during microscopic testing. They achieved satisfactory levels of mechanical characteristics, such as tensile and hardness [16, 17]. The weld was found to be broken up to 201 MPa [18]. A variety of titanium-stainless steel laser welding combinations are being studied, and the result shows that the combination is not practicable because of the weld's embrittlement. Interlayers in the form of tantalum strips have been gradually increasing the joint's strength [19-22]. With a 2.5 kW CO_2 laser and helium shielding gas, the laser dissimilar butt joint of magnesium alloys was successfully completed. Observations of microstructures in the fusion zone showed that recrystallization was going in the right direction. For the joints' microhardness distribution, there were no significant effects across the profile [23-28].

 https://doi.org/10.37896/pd91.4/91419

ISSN: 0369-8963

An Nd: YAG laser was used to fuse incompatible stainless steel butt joints together. It was determined that the tensile strength and weld breadth On the other hand, for a given parametric condition, the 304SS base material has better microstructural and mechanical qualities than the 316SS. Finally, desirability function analysis has been used for multi-objective optimization in order to maximise ultimate tensile strength and minimise weld width simultaneously [29]. A 500W Nd: YAG laser lap joint made of austenitic stainless steel and nickel-based super alloy.The joints were analysed using microstructure, tensile, and microhardness. At the weld junction, a tensile fracture occurred, reducing the strength and hardness of the base metal by 17% [30, 31]. An austenitic stainless steel 304 butt junction was studied using a factorial approach to predict weld bead geometry. They came to the conclusion that input process factors have both direct and indirect effects on the shape of our weld beads [32].The crack propagation and micro hardness distribution were studied in laser welded 316 steel, which had better qualities than the basic metal. In order to conduct the experiment, CO_2 laser welding was used to weld the parts together. However, two different thicknesses of high-strength steel, 1.6 mm and 2.0 mm, The process accuracy was examined in great depth, and the laser welding procedure was able to combine even the most complex of materials [33]. The weld bead profile and the heat-affected zone were analysed for P92 (Cr–W–Mo–V) steel. The joining process was optimised by employing a CO_2 laser welding machine. Micro-harndess and microstructure studies show that laser welding is accurate and can be done in the real world [34].

The microstructure and mechanical characteristics of the welding of Fe-Cu using a continuous CO_2 laser The two sides of the weld produced different microstructural results. The iron side aided in the modification of characteristics in response to adjustments in process parameters. The weld zone has a higher hardness value than the other base metals.Weld zone hardness is raised because of Fe and Cu fine grain zones [35, 36]. A fibre laser welding technique was used for the weld of SS and low-carbon steel dissimilar joints. The dissimilar joint's quality and the weld bead shape and weld area were the outputs of the optimization process. Dissimilar metal laser welding requires a high level of laser power in order to achieve a strong weld [37]. Stainless steel AISI430F and AISI440C are laser welded together to form a new joint. For the prevention of the production of cracks, post-heat treatment and preheat treatment have been utilized. The weld zone's material parameters were determined by

 https://doi.org/10.37896/pd91.4/91419

ISSN: 0369-8963

conducting a microstructure investigation. In the fusing area, martensite and ferrite structures formed as a result of the outcomes. A microhardness test shows that the hardness of the fusion zone is much higher than that of the base metal [38].

SS316 and Nickel dissimilar junctions without filler wire have not been documented in the open literature, which accounts for the problem. As a result of this work, the mechanical properties of laser beam welded dissimilar joints were predicted. A macro and microstructural study of the weld joint is presented. Tests on dissimilar welding of stainless steel plate and nickel plate of 5 mm thickness were carried out.

Experimental Procedures

Laser Welding Process and Materials

Figure 1. Experimental Setup of the TRUMPF LASERCELL TLC1005

Table 1 shows the chemical compositions of the base metals used for welding dissimilar metals of SS 316 and Nickel 201. Butt-joint welding is used to link AISI 316 stainless steel with commercially pure nickel plates. Fig.1 shows the laser machining centre used to weld the butt joint, which has a maximum output power of 4 kW and a laser beam diameter of 0.5 mm. Figure 1 depicts the components of the experiment, and Table 2 indicates the experimental conditions and numerous parameters employed in the joining method. There is 15 lpm of argon shielding gas flowing through the nozzles. Bead on plate (BOP) and extensive trial runs are used to discover the process parameters. The Fe and Ni plates have a thickness of 5.0 mm.

 https://doi.org/10.37896/pd91.4/91419

ISSN: 0369-8963

Table 1. Chemical Composition of Stainless Steel 316 L with Nickel 201 (mass fraction, %)

	Fe	Si	C	Cr	Mn	Ni
SS 316 L	Bal.	0.90	0.02	18.50	1.70	11.50
Ni 201	0.40	0.35	0.02	--	0.35	Bal.

Figure 2. Beads on the Plate and Weld Sample Trials.

Table 2. The Process Parameters for Welding Techniques.

Process parameters	**Values**
Laser power (W)	2790, 3210
Speed (mm/min)	625, 975
Position of laser beam	0.15 mm offset towards Nickel side
Focal length (mm)	200 mm
Laser beam angle	87^0
Gas flow rate (lpm)	15
Focal position	-0.75 from the surface

Characteristics of Joints

An EDM wire cutter was used to fabricate the welded specimen for ASTM E8-16a and perform the tensile test on the Unitek 9450 Electro-Mechanical Universal Testing Machine. A standard specimen size of ASTM E384-16 was used with a Matsuzawa-MMTX7 Microhardness Tester (Make/Model) to test the hardness.

The sample was cut across the weldment and polished with a series of emery papers ranging from 100 to 1000 grit sizes for metallographic inspection. A diamond paste 1-2 microns

 https://doi.org/10.37896/pd91.4/91419

ISSN: 0369-8963

in size was used to lap it. The etching was done using Aquaregia and Marble's reagents in a masking technique. The investigation was carried out with the help of an optical metallurgical microscope (Zeiss, AxioVert. A1). A stereomicroscope with a 10x magnification was used for the macro inspection. MACSCOPE-Z and Pixel Fox Camera are used to measure the weld bead profile (dhs Imaging System, Ver. 6.02, Germany).

Results and Discussions

Micro and Macrostructures

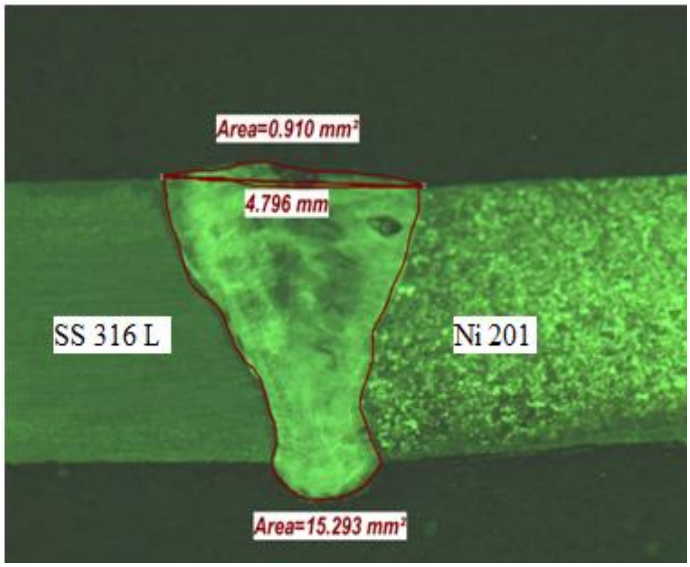

Figure 3. Sample Weld Pool Measurements.

The macrostructures of the samples are used to measure the weld profile dimensions. According to the research, the average weld pool has an area of 12.14 mm^2 and an average weld thickness of 3.38 mm, with 4.54 mm being the average weld penetration depth. Figure 3 depicts the macro investigation and the related measurements. Nickel 201 microstructure images of Fig.4 (a) display large, equiaxed gamma (nickel) solid solution grains. At the grain borders, no carbide precipitation can be seen, and annealing twins can be found within the grains themselves. In the microstructure image of stainless steel SS 316 L shown in Fig.4(b), fine austenite grains can be seen within the annealing twins, and there is less than 5% free ferrite. Fine nickel solid solution dendrites are visible in the microstructure image indicated in Fig. 4 (c). The interdendritic area

 https://doi.org/10.37896/pd91.4/91419

ISSN: 0369-8963

has some delta ferrite and the structure of the solidified matter is clearly visible. It's a good mix, and the weld appears to have some porosity.

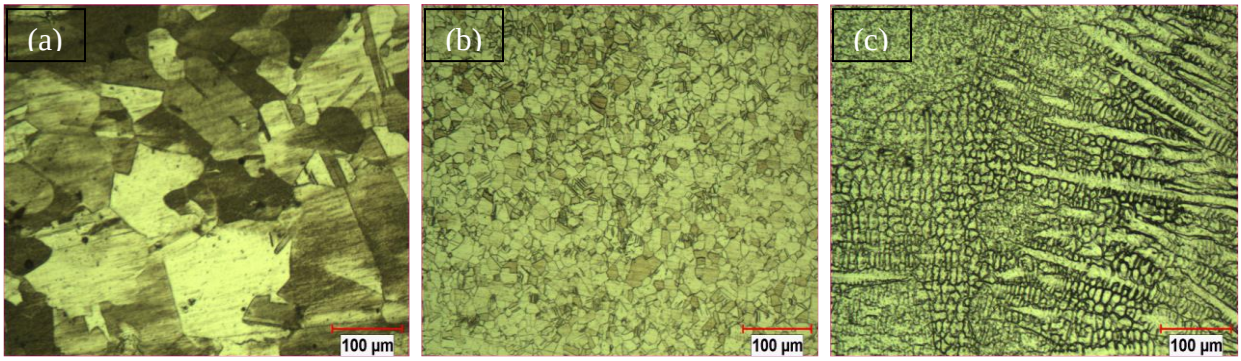

Figure 4. (a) Microstructure of Nickel 201 Base Metal (b) Microstructure of Stainless Steel 316L Base Metal (c) Microstructure of Weld.

Micro-hardness of the Material

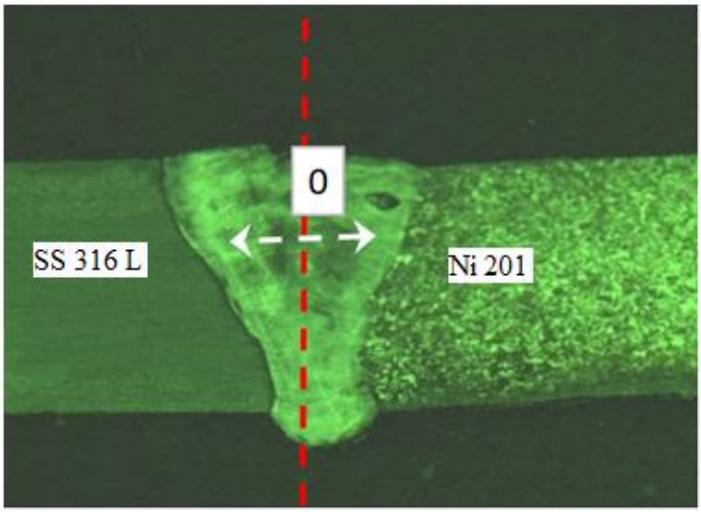

Figure 5. Micro-hardness Survey in Sample 4.

As shown in Fig. 5, micro-hardness measurements across the weld are used to identify the tensile properties of the weld. The micro-hardness profile of sample 4 is depicted in Fig. 6. Based on the measured values, high levels of micro-hardness throughout the fusion border and no substantial rise in the melted zone were discovered, as well as a progressive drop towards the nickel region. Nickel 201 is 138 to 157 VHN and SS 316 L is 200 to 243 VHN. Due to laser welding's minimal heat input and extremely high power densities, there is no change in hardness at the fusion line in the base metals, confirming that HAZ is not an issue [39].

 https://doi.org/10.37896/pd91.4/91419

ISSN: 0369-8963

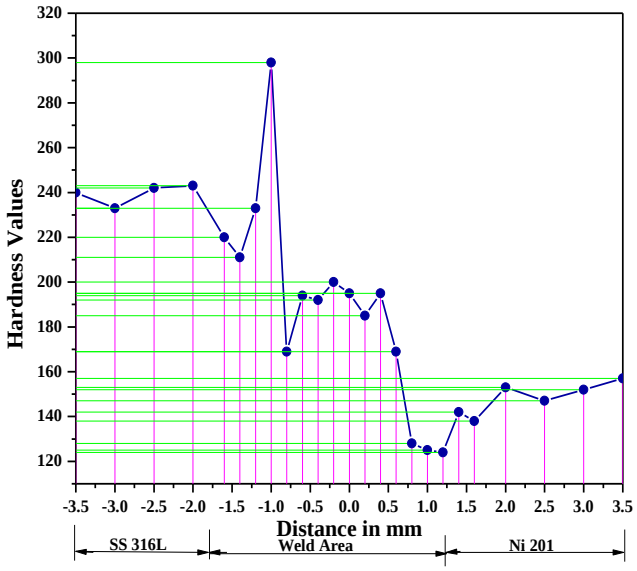

Figure 6. Microhardness Profile of Welded Sample 4.

Tensile Strength

Table 3. The Tensile Strength of the Test Samples.

Sample	Tensile stress (MPa)	Fracture Location
1 (2790 W, 625 mm/min.)	284	Weld
2 (2790 W, 975 mm/min.)	405	Closer to weld at Ni 201
3 (3210 W, 625 mm/min.)	398	Closer to weld at Ni 201
4 (3210 W, 975 mm/min.)	412	Parent metal (Nickel 201)

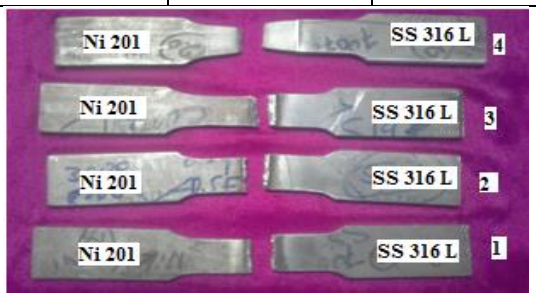

Figure 7. The Fractured Welding Samples of Ni 201 and SS 316 L.

https://doi.org/10.37896/pd91.4/91419

ISSN: 0369-8963

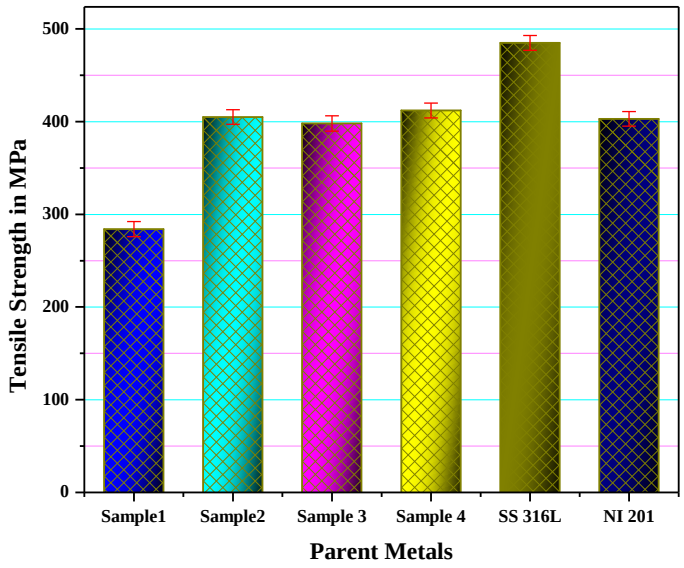

Figure 8. A Comparison of Tensile Strength of the Samples with Parent Metals.

Figure 7 depicts the broken specimens from tensile testing performed on four welded test specimens. The results demonstrate that the weld strength for sample 4 is virtually similar to the base metal nickel 201, as shown in Fig. 8. This is likewise the case for samples 2 and 3. Although the tensile results are acceptable, sample 2 is not. Nodules may have caused nickel 201 samples 2 and 3 to break because of the voids in their HAZ. No cracks were discovered in the weld region in any of the samples. Due to an underfill problem, weld sample 1 fails. Underfill fault is caused by high power and low speed, as seen in Fig. 9 (a). In contrast to sample 1, which had an underfill defect, sample 2 was free of porosities yet was welded at the same power. Weld samples in fig. 9 (b), (c), and (d) have cumulative porosity values of 0.931 mm, 2.712 mm, and 0.632 mm, respectively. Porosity can also be minimised by controlling the power and speed at which the material is processed [40, 41]. The porosity values in sample 4 are good because they are lower than those in samples 1 and 2.

https://doi.org/10.37896/pd91.4/91419

ISSN: 0369-8963

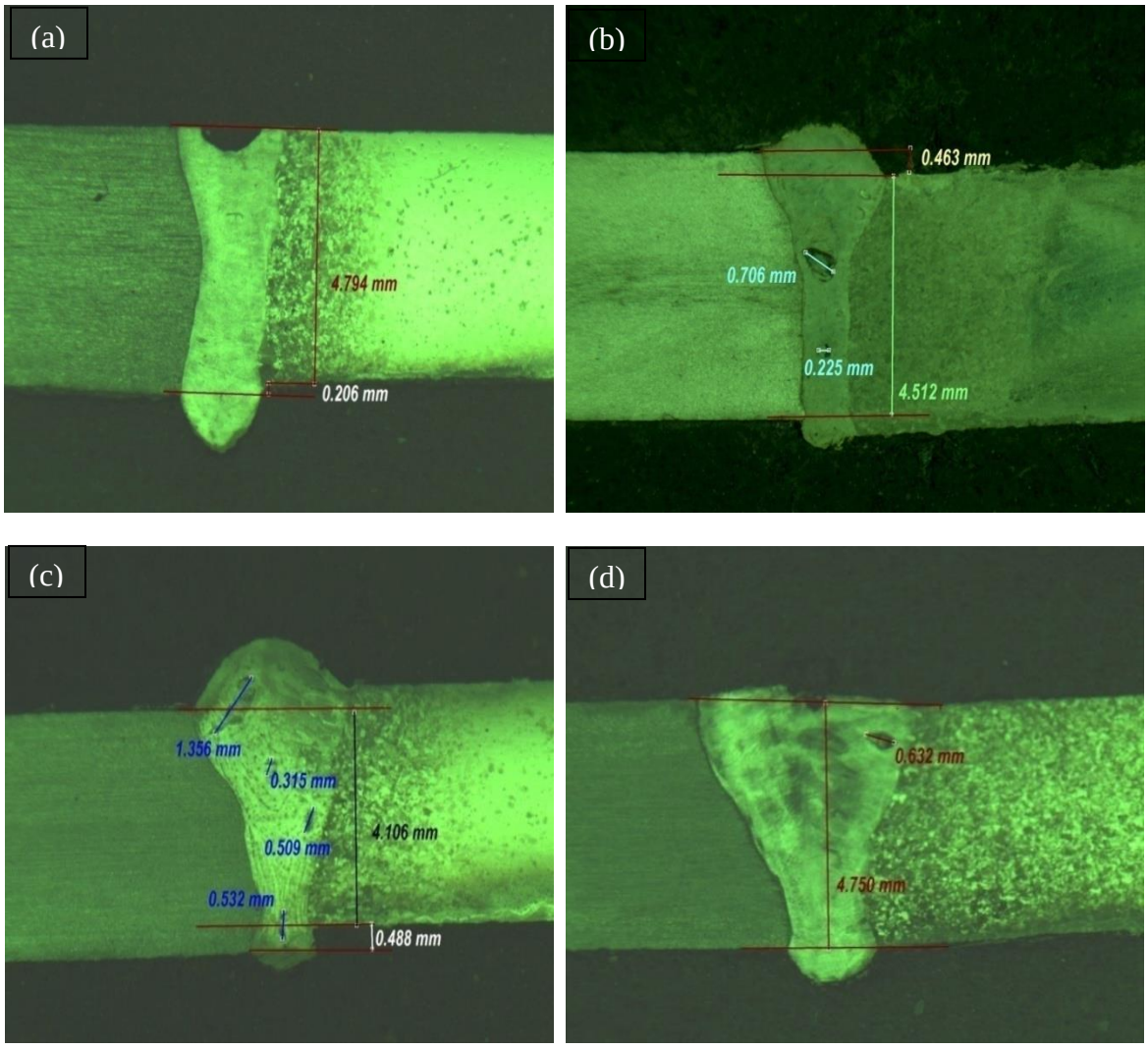

Figure 9. Micro Structures of Various Samples (a) Weld Sample 1 (b) Weld Sample 2 (c) Weld Sample 3 (d) Weld Sample 4.

Conclusions

The dissimilar metal welding was performed on nickel 201 and stainless steel 316 L plates of 5 mm thickness by CO_2 laser welding without filler metal. From this study, we can draw the following conclusions:

- Welding of dissimilar metals of SS316L and nickel 201 using CO_2 lasers and no filler metal with an acceptable tensile strength of more than 412 MPa has been successfully accomplished.

 https://doi.org/10.37896/pd91.4/91419

ISSN: 0369-8963

- Weld joints between incompatible metals are shown to have a columnar structure by macro and microstructure analyses, indicating successful fusion. Weakness characteristics are influenced by manufacturing parameters like porosity and underfill flaws.

- No considerable amount of HAZ can be seen in the micro-hardness profile of the successful sample 4 specimen. Acceptable micro-hardness levels in the weld zone allow for a smooth transition from SS 316 L through the fusion zone to Nickel 201.

References

[1]. Jose Roberto Berretta., Wagner de Rossi., Mauricio David., Martins das Neves., Ivan Alves de Almeida., and Nilson Dias Vieira Junior. 2007. Pulsed Nd:YAG laser welding of AISI 304 to AISI 420 stainless steels. *Optics & Laser Technology* 45: 960-s to 966-s.

[2]. Anton Evdokimov., Nikolay Doynov., Ralf Ossenbrink., Aleksei Obrosov., Sabine Weiß., and Vesselin Michailov. 2021. Thermomechanical laser welding simulation of dissimilar steel-aluminum overlap joints. *International Journal of Mechanical Sciences* 190: 106019.

[3]. Jun Dai., Banglong Yu., Wei Jiang., Hla Min Htun., and Zheng Liu. 2019. Laser Welding of Dissimilar Metal Joint of 6061 Al Alloy and Al Matrix Composite. *Advances in Materials Science and Engineering* 2359841.

[4]. T. M. Yue., J. H. Xu., and H. C. Man. 1997. Pulsed Nd-YAG Laser Welding of A SiC Particulate Reinforced Aluminium Alloy Composite. *Applied Composite Materials* 4: 53-s to 64-s.

[5]. Massaud Mostafa., J. Laifi., M. Ashari., and Z.A. Alrowaili. 2020. MATLAB Image Treatment of Copper-Steel Laser Welding. *Advances in Materials Science and Engineering* 8914841.

[6]. Jae-Do Kim., Cheol-Jung KIM., and Chin-Man Chung. 2001. Repair welding of etched tubular components of nuclear power plant by Nd:YAG laser. *Material Processing Technology* 114: 51-s to 56-s.

 https://doi.org/10.37896/pd91.4/91419

ISSN: 0369-8963

[7]. A. Angelastro., S.L. Campanelli., and G. Casalino. 2015. Study on welding–brazing of copper and stainless steel using tungsten/metal gas suspended arc welding. *Materials Letters* 156: 7-s to 9-s.

[8]. R.S.Parmar. 1997. *Welding processes and technology*, Khanna Publishers.

[9]. Bao Chen., Sun Yongduo., Wu Yuanjun., Wang Kaiqing., Wang Li., and He Guangwei. 2020. Fracture properties and crack tip constraint quantification of 321/690 dissimilar metal girth welded joints by using miniature SENB specimens, *Nuclear Engineering and Technology*, https://doi.org/10.1016/j.net.2020.12.020

[10]. Sergey Kuryntsev. 2022. A Review: LaserWelding of Dissimilar Materials (Al/Fe, Al/Ti, Al/Cu)—Methods and Techniques. Microstructure and Properties, *Materials* 15: 122.

[11]. E.M. Anawa., and A.G. Olabi. 2008. Control of welding residual stress for dissimilar laser welded material. *Material Processing Technology* 204: 22-s to 33-s.

[12]. Dawes. C., 1997. *Laser welding*, First edition, Abington Publications.

[13]. Youwei Xu., and Xuqian Hou. 2021. Correlation between the microstructure and corrosion behaviour of copper/ 316L stainless-steel dissimilar-metal welded joints. *Corrosion Science* 191: 109729.

[14]. Ali Yürük., Bekir Çevik., and Nizamettin Kahraman. 2021. Analysis of mechanical and microstructural properties of gas metal arc welded dissimilar aluminum alloys (AA5754/AA6013). *Materials Chemistry and Physics* 273: 125117.

[15]. Yu Zhang., Zhipeng Cai., Chaoyu Han., Xin Huo., Manjie Fan., Kejian Li., and Jiluan Pan. 2021. Macrosegregation induced interface structure and its effect on creep failure in dissimilar metal welds between Ni-based alloy and 10% Cr martensitic steel. *Materials Science & Engineering A* 824: 141847.

[16]. Tobias Solchenbach., and Peter Plapper. 2013. Mechanical characteristics of laser braze-welded aluminium copper connections. *Optics & Laser Technology* 54: 249-s to 256-s.

 https://doi.org/10.37896/pd91.4/91419

ISSN: 0369-8963

[17]. Zhenghua Meng., Rui Zhou., Mengyuan Gong., Wei Guo., Wei Liu., and Shangyu Huang. 2021. Interface formation and interlayer factors of three-dissimilar-metal layers joint in impact welding. *Journal of Manufacturing Processes* 70: 414-s to 426-s.

[18]. K.W.Carlson. 1985. Proceedings of International Congress on application of Lasers and Electro Optics 49-s to 57-s.

[19]. Bikash Ranjan Moharana., Sushanta Kumar., and Sahua Susanta Kumar, Sahoo Ravi Bathe. 2016. Experimental investigation on mechanical and microstructural properties of AISI 304 to Cu joints by CO_2 laser. *Engineering Science and Technology* 19: 684-s to 690-s.

[20]. Khot Rahul, S., and Venkateswara Rao, T. 2020. Investigation of Mechanical Behaviour of Laser Welded Butt Joint of Transformed Induced Plasticity (TRIP) Steel with effect Laser Incident Angle. *International Journal of Engineering Research and Technology* 13(11): 3398-s to 3403-s.

[21]. Yan Zhang., Yan Kun Chen., Jian Ping Zhou., Da Qian Sun., and Hong Mei Li. 2020. Laser Welding of TC4 Ti Alloy and 304 Stainless Steel with Different Joining Modes. *International Journal of Metallurgy and Metal Physics* 5: 055-s to 62-s.

[22]. Zhongmei Gao., Xinyu Shao., Ping Jiang., Longchao Cao., Qi Zhou., ChenYue., Yang Liu., and Chunmin Wang. 2016. Parameters optimization of hybrid fiber laser-arc butt welding on 316 L stainless steel using Kriging model and GA. *Optics & LaserTechnology* 83:153-s to 162-s.

[23]. D. Parkes., W. Xu., D. Westerbaan., S.S. Nayak., Y. Zhou., F. Goodwin., S. Bhole., and D. L. Chen. 2013. Microstructure and fatigue properties of fiber laser welded dissimilar joints between high strength low alloy and dual-phase steels. *Materials and Design* 51: 665-s to 675-s.

[24]. Roshith, P. 2021. Enhancement of metallurgical and mechanical properties of the materials by performing CO_2 Laser beam welding. *Welding International* DOI: 10.1080/09507116.2021.1959272

 https://doi.org/10.37896/pd91.4/91419

[25]. M. Palanivendhan., J. Chandradass., Devansh Nagpal., and Manas Tiwa. 2020. Mechanical Characterization of dissimilar metal welding of SS 202 & SS 409 by ND-YAG laser welding. *PalArch's Journal of Archacology of Egyht/ Egyptology* 17(7): 7182-s to 7194-s.

[26]. Xian-Rong Zhou., Jie Ning., Suck-Joo Na., and Lin-Jie Zhang, 2021. Microstructures and properties of the dissimilar joint of pure molybdenum/T2 copper by single-mode laser welding. *International Journal of Refractory Metals and Hard Materials* 101: 105667.

[27]. H. Eisazadeh., and D.K. Aidun. 2021. Residual stress reduction in dissimilar metals weld. *Journal of Manufacturing Processes* 64: 1462-s to 1475-s.

[28]. Yufeng Zhang., JihuaH uang., Hai Chi., Nan Cheng., Zhi Cheng., and Shuhai Chen. 2017. Statistical analysis and optimization of direct metal laser deposition of 227-F Colmonoy nickel alloy. *Optics and Laser Technology* 94: 138-s to 145-s.

[29]. B. Shanmugarajan., and G. Padmanabham. 2012. Fusion welding using laser on Ti-SS dissimilar combination. *Optics & Laser Technology* 50: 1621-s to 1627-s.

[30]. Pawel Kolodziejczak., and Wojciech Kalita. 2009. Properties of CO_2 laser-welded butt joints of dissimilar magnesium alloys. *Journal of materials processing technology* 209: 1122-s to 1128-s.

[31]. R. Rajkumar., N. Gnana Prasanna., and F. Michael Raj. 2020. Experimental Investigation of Wire EDM Process Parameters on SiC Particles Reinforced AA6063 (Black & Green) Aluminium Alloy Matrix Composites. *Tierärztliche Praxis* 40: 1819-s to 1834-s.

[32]. Nikhil Kumar., Manidipto Mukherjee., and Asish Bandyopadhyay. 2017. Study on laser welding of austenitic stainless steel by varying incident angle of pulsed laser beam. *Optics & Laser Technology* 88: 24-s to 39-s.

[33]. Siyu Zhou., Dongsheng Chai., Jingling Yu., Guangyi Ma., and Dongjiang Wu. 2017. Microstructure characteristic and mechanical property of pulsed laser lap-welded nickel-based superalloy and stainless steel. *Journal of Manufacturing Processes* 25: 220-s to 226-s.

 https://doi.org/10.37896/pd91.4/91419

ISSN: 0369-8963

[34]. K. Manonmani., N. Murugan., and G. Buvanasekaran. 2007. Effects of process parameters on the bead geometry of laser beam welded stainless steel sheets. *Advanced Manufacturing Technology* 32: 1125-s to 1133-s.

[35]. S.A. Fabritsiev., D. Kiselev., and A.A. Kazakov. 2018. Investigations of the mechanical properties and structure of laser welds for ITER divertor and first wall. *Fusion Engineering and Design* 127: 139-s to 150-s.

[36]. R, Rajkumar., N, Gnana Prasanna., and F, Michael Raj. 2019. Influence of Processing Parameters on AA 6063/SiC (Black & Green) Composites in Wire EDM. *Caribbean Journal of Science* 53(2): 1966-s to 1990-s.

[37]. Young Whan Park., Hyunsung Park., Sehun Rhee., and Munjin Kang. 2002. Real time estimation of CO_2 laser weld quality for automotive industry. *Optics & Laser Technology* 34: 135-s to 142-s.

[38]. Shanmugarajan, B., Rishabh Shrivastava,, Sathiya, P., and Buvanashekaran, G. 2016. Optimisation of laser welding parameters for welding of P92 material using Taguchi based grey relational analysis. *Defence Technology* 12: 343-s to 350-s.

[39]. Gandham Phanikumar., Sambandam Manjini., Pradip Dutta., Jyotirmoy Mazumder., and Kamanio Chattopadhyay. 2005. Characterization of a continuous CO_2 laser-welded Fe-Cu dissimilar couple. *Metallurgical And Materials Transactions A* 36: 2137-s to 2147-s.

[40]. Yuewei Ai., Xinyu Shao., Ping Jiang., Peigen Li., Yang Liu., and Wei Liu. 2016. Welded joints integrity analysis and optimization for fiber laser welding of dissimilar materials. *Optics and Lasers in Engineering* 86: 62-s to 74-s.

[41]. M.M.A. Khann, L. Romoli., and G. Dini. 2013, Laser beam welding of dissimilar ferritic/martensitic stainless steels in a butt joint configuration. *Optics & Laser Technology* 49: 125-s to 136-s.

.

 https://doi.org/10.37896/pd91.4/91419